

Time-resolved splitting of magnons into vortex gyration and Floquet spin waves

T. Devolder,^{1,*} R. Lopes Seeger,¹ C. Heins,² A. Jenkins,³ L. C. Benetti,³ A. Schulman,³ R. Ferreira,³ G. Philippe,¹ C. Chappert,¹ H. Schultheiss,² K. Schultheiss,² and J.-V. Kim¹

¹*Université Paris-Saclay, CNRS, Centre de Nanosciences et de Nanotechnologies, Palaiseau, France*

²*Helmholtz-Zentrum Dresden-Rossendorf, Dresden, Germany*

³*International Iberian Nanotechnology Laboratory, Braga, Portugal*

(Dated: November 14, 2025)

Forced excitations at frequencies in the range of the first order azimuthal spin waves of a magnetic disk in the vortex state are known to scatter into the vortex gyration mode, thereby allowing the growth of Floquet spin waves forming a frequency comb. We study the temporal emergence of this dynamical state using time-resolved microwave electrical measurements. The most intense Floquet mode emerges synchronously with the gyration mode after a common incubation delay which diverges at the scattering threshold. This delay is minimal when the drive is resonant with one of the first order azimuthal spin waves. It can be as short as 3 ns for the maximum investigated power. We conclude that the first-to-occur scattering mechanism is the three-wave splitting of a regular azimuthal eigenmode into a coherent pair formed by a gyration magnon and a Floquet spin wave.

INTRODUCTION

Magnetic disks having a vortex ground state have become a popular system both for magnonics applications [1] and as model test bench for micromagnetic theories [2, 3]. Their eigenspectrum comprises a low frequency mode –the translational motion of the vortex core, most often referred to as the gyration mode–, as well as the confined spin wave modes that have frequencies higher by typically more than one order of magnitude [4]. The high frequency modes are conveniently described by a radial index n and an azimuthal index m , that respectively count the number of nodes along the disk radius and in the azimuthal direction along half a perimeter, respectively.

The magnetization of vortex dots is easily set in the non-linear regime where spin waves start to scatter mutually [5–8] and interact with the vortex core. The interactions between the core and spin waves have been studied along two main lines. The hybridization of the azimuthal spin waves with the gyration mode [9, 10] was first shown to lift the degeneracy between spin waves of opposite azimuthal indices [9, 11]. In parallel, active research was conducted on the possibility to switch the polarity of the vortex core by interaction with azimuthal spin waves [12, 13], sometimes in conjunction with an active pumping of the gyration [14].

Together with these two regimes, interactions between the high frequency spin waves and the vortex core are occurring [15]. This was studied numerically. Z. Gao et al. [16] analyzed the reaction of the vortex core to an impinging spin wave beam. They showed that in addition to the forced excitation due to the incoming wave, core gyration is induced and the excitation spectrum splits into a frequency comb with finger spacing being the gyration frequency. Z. Wang et al. [17] proposed that the physical origin of such frequency comb is the confluence

and splitting scattering of $m = 1$ azimuthal spin waves with the gyration mode of the vortex core. The emergence of the frequency comb was then confirmed experimentally by C. Heins et al. [18, 19]. In addition, Heins et al. showed that the high frequency modes involved in the scattering are not the regular eigenmodes of the system but rather magnon Floquet states constructed on the time-periodic gyrating vortex, and populated by the nonlinear coupling of driven magnon modes to the vortex core gyration. These earlier works [18–20] provided a clear understanding of the steady state situation and its event-averaged transient but did not dig into the dynamics of how azimuthal spin wave modes scatter into vortex core gyration and how they adapt to the resulting Floquet context. Since scattering is most often a stochastic process, some features of this process can only be revealed by real-time single-shot experiments.

In this paper, we build on the works of ref. [18–20] and study the transient response of a vortex dot to in-plane rf magnetic fields of frequency close to that of the azimuthal spin wave modes. Time-resolved, high sensitivity measurements are enabled thanks to the embedding of the vortex dot in a magnetic tunnel junction. This embedding is an important step towards potential future applications, i.e. frequency down conversion; it allows us to elucidate the spin wave scattering mechanism that triggers the genesis of the Floquet spin waves.

We work with 45-nm-thick circular magnets made from a CoFeBSi alloy with a vortex ground state. We studied magnets of diameters ranging from 200 to 1000 nm, with typically 10 devices per diameter. The magnets are embedded in magnetic tunnel junctions (MTJs) of magneto-resistance 180% and resistance of typically $320\ \Omega$ for a diameter of 300 nm. The reference layer is uniformly magnetized and fixed. The MTJs and their contact pads are small enough to be considered as lumped elements, with electrical bandwidth exceeding 20 GHz. The spin fluctu-

ations within the magnet are studied by sensing the voltage V that the MTJ delivers to an amplifier equivalent to a 50Ω load [Fig. 1(a)]. This voltage is either analyzed in frequency domain using a spectrum analyzer of resolution bandwidth set to 2 MHz or time-resolved using a single-shot oscilloscope. The measurements are sensitive to the spin excitations that result in variations δR of the MTJ resistance. Because of the symmetry of our system, the largest δR 's correspond to magnetization fluctuations of first order azimuthal symmetry; this includes the vortex gyration and the spin waves with azimuthal indices [21, 22] $m = \pm 1$. Our sensitivity to other modes is small (but finite) and depends on the exact mode profile and how the space-resolved magneto-conduction dynamically redistributes the current across the MTJ as a response to this profile [23].

Without any other excitation except the thermal fluctuations, δR can already be revealed by dc biasing (current I_{dc} from a bias of ± 200 mV) the MTJs and measuring the spectral density $||\tilde{V}(f)||^2$ of the voltage that the MTJ delivers [Fig. 1(b)]. This spectrum contains discrete lines well-described by the expected $\chi''(f)/f$ shape [24] where $\chi''(f)$ is a Lorentzian function. The main fluctuation is at 597(26) MHz and it is ascribed to the gyration mode [25]. The frequencies of the other main fluctuators are 4.13(170) GHz, 5.49(240) GHz and 7.0(≈ 300) GHz, where the numbers in parentheses are the FWHM linewidths in MHz. We believe that the mode at 4.13 GHz belongs to the fixed layer of the MTJ and, as it will not react to the rf stimuli we shall disregard it from now on. While the frequency of the gyration mode varies by ± 70 MHz from device to device as a result of material granularity [26], the other ones are reproducible. Spin waves of higher frequencies are also thermally active; they lead to a broad spectral feature in the 8-10 GHz interval [Fig. 1(b)] that plays no role in our study.

We performed `Magnum.np` eigenmode simulations [27] using the measured magnetization ($M_s \approx 500$ kA/m) and an estimated exchange stiffness of 10 pJ/m. The predicted eigenmodes include the gyration mode of frequency $f_g = 585$ MHz, and confined spin wave modes of frequencies $f_{n=0, m=-1} = 5.9$ GHz, $f_{n=0, m=+1} = 7.45$ GHz and $f_{n=1, m=-1} = 8.64$ GHz mode. The sign of the azimuthal indices m of the spin waves are given assuming a vortex core of positive polarity. The $\{n = 0, m = +1\}$ mode has a thickness profile indicating some hybridization with the flexural gyration mode [28]. Small variations of the assumed material parameters and device size affect the frequencies of the modes, but not their frequency sequence. Owing to the reasonable numerical agreement, we assign the $\{n = 0, m = -1\}$ and the $\{n = 0, m = +1\}$ modes at 5.9 and 7.45 GHz to their experimental counterparts at 5.49 and 7.0 GHz. As from now on we shall only deal with $n = 0$ modes, we will omit this index and quote these modes as $|g\rangle$, $|m = -1\rangle$ and

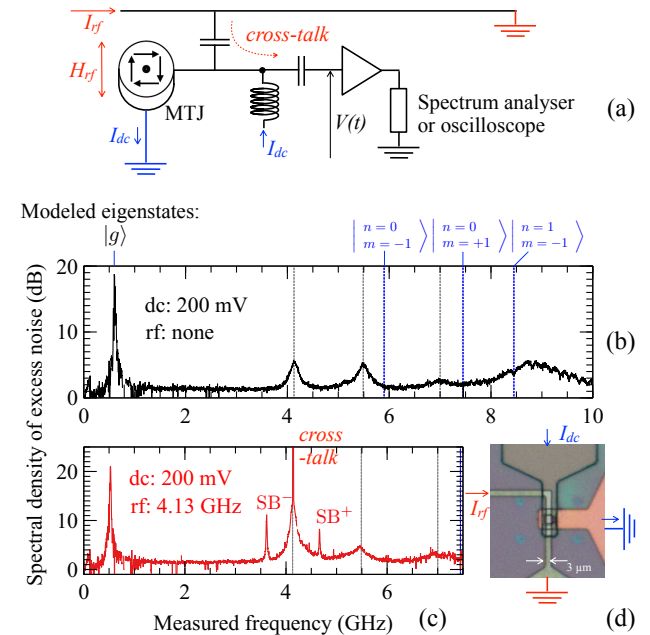


FIG. 1. Set-up and effect of the dc and rf drives in the linear regime. (a) A wire fed with an rf current applies a field on a circular magnet in the vortex state. The magnet is part of a magnetic tunnel junction which delivers a voltage $V(t)$ to the measuring instruments. (b) Thermal spin waves (grey lines): Increase of the power spectral density of V when changing the dc bias from 0 to 200 mV. The blue lines are the frequencies of the modes of azimuthal indices $m = \pm 1$ in the micromagnetic simulations. (c) Spectrum with the signal of thermal spin waves, cross-talk signal and microwave mixing signal leading to the sidebands SB^- and SB^+ when applying an rf drive at 4.13 GHz and 10.8 dBm. (d): Optical micrograph of a device.

$|m = +1\rangle$.

Each MTJ is placed $1.2 \mu\text{m}$ below a $3 \mu\text{m}$ -wide metallic line [Fig. 1(d)] connected to an rf source that supplies a fast rising (< 100 ps) rf current I_{rf} of adjustable frequency f_{rf} [Fig. 1(a)]. The generated rf field is of the order of 1 mT for 2.8 dBm of power arriving at the field line. It has three effects.

- (i) First, it unavoidably generates a parasitic cross-talk responsible for the most intense peak in the $||\tilde{V}(f)||^2$ spectra, right at f_{rf} , as in the example of Fig. 1(c).
- (ii) Second, I_{rf} generates an in-plane rf magnetic field. The layout of the sample ensures that the rf field is uniform at the scale of the vortex disks. This rf field is assumed not to actuate the magnetically-hard reference layers of the MTJ. Conversely, this rf drive induces a forced excitation of the magnet, excitation that we shall simply quote as $|rf\rangle$. By symmetry, the excitations with azimuthal symmetry $m = \pm 1$ (including the gyration) are much more excited than any other ones [22]. The created population of $|rf\rangle$ yields a resistance fluctuation δR at the frequency f_{rf} . This should in principle be seen as an additional signal at f_{rf} in the spectra when a dc cur-

rent biases the junction. Unfortunately the signal generated by this forced excitation is hidden below the cross-talk [29]. So, the value $\|\tilde{V}(f = f_{\text{rf}})\|^2$ is unfortunately not magnetically informative.

(iii) Third, the interplay between the rf current and the magnetization fluctuations generates frequency mixing. Indeed, if the resistance fluctuates by δR_{fluct} at a frequency f_{fluct} this modulates the amplitude of the voltage across the MTJ. This leads to two sidebands (SB⁺ and SB⁻) at the frequencies $f_{\text{rf}} \pm f_{\text{fluct}}$, each carrying a power:

$$P_{\text{SB}} \propto \delta R_{\text{fluct}} \cdot I_{\text{rf}}^2 \quad (1)$$

and having a linewidth reflecting that of the fluctuator. In practice the gyration mode is *always* (at least thermally) populated so that two mixing sidebands (SB⁻ and SB⁺) are bound to *always* appear at $f_{\text{rf}} \pm f_g$. Fig. 1(c) is an illustration of this mixing-induced sidebands. For the parameters of [Fig. 1(c)], i.e. the drive being at 4.13 GHz, the rf field induces a linear response, so that the spectral signatures of the (thermally populated) regular eigenmodes just add to the effect of the drive [Fig. 1(c)]. These mixing-induced sidebands are still present if the dc bias is suppressed (not shown).

We emphasize that in the linear regime this frequency mixing yields *only the first* lateral sidebands while the cross-talk yields an additional peak at f_{rf} . The spectrum is thus trident-like [see Fig. 1(c)] and by no means this amplitude modulation effect could generate a frequency comb.

We have stayed so far in a low amplitude regime for which there is no scattering among spin waves. Studies in comparable vortex disks [18] showed that when sufficiently populated, the spin waves scatter into the gyration mode, and in this case, the large gyration can create a Floquet context that renormalizes the spin wave manifold. Being electrical and broadband, our setup can conveniently study the temporal evolution of this phenomenon.

Fig. 1(c) showed that when f_{rf} was tuned to 4.13 GHz the forced mode $|\text{rf}\rangle$ was not scattering. We confirmed that when the same conditions are used but f_{rf} is increased to a value closer to $f_{m=-1}$, the system abruptly transits into a completely different dynamical regime in which the device delivers a substantially larger power at the gyration frequency with profoundly modified spectral features at higher frequencies, including a high frequency comb. Meanwhile the coherence of the gyration also improves so that higher harmonics of the gyration frequencies appear. Fig. 2 reports an example of the total power emitted by the gyration (arbitrarily defined as $\int_{10 \text{ MHz}}^{1 \text{ GHz}} \|\tilde{V}(f)\|^2 df$) versus the frequency f_{rf} and power of the drive. The appearance of the strong gyration signal is accounted for by the well-defined bright tongue which is rather symmetric about $f_{m=-1}$. This confirms that

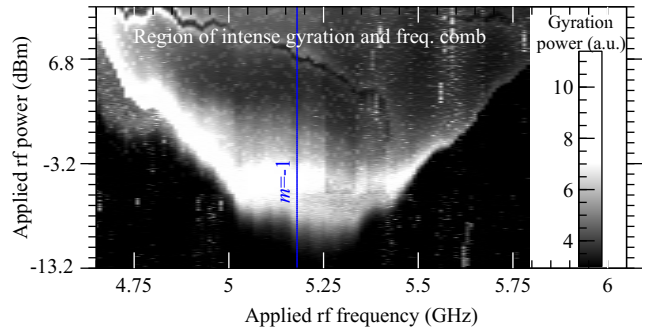


FIG. 2. (c) Total power of the gyration mode (defined as $\int_{10 \text{ MHz}}^{1 \text{ GHz}} \|\tilde{V}(f)\|^2 df$) versus stimulus power and drive frequency f_{rf} for a bias of 200 mV on a device of diameter 400 nm, whose $m = -1$ regular mode is at 5.18 GHz (vertical blue line). The black color level corresponds to the power generated by the thermal fluctuations of the gyration.

the forced mode $|\text{rf}\rangle$ scatters into the gyration mode $|g\rangle$. Such transition was observed in all the investigated devices (i.e. for all diameters in the 200 nm to 1 μm range) provided the drive frequency is tuned to their proper frequencies.

Fig. 3(a) shows that there appears concurrently an additional frequency comb centered about the drive frequency and spanning the values $f_{\text{rf}} + kf_g$, with $k \in \mathbb{Z}$. The sideband SB⁻ (i.e. $k = -1$) is systematically the most intense one after the (cross-talk dominated) peak at the drive frequency. This could have been expected since the scattering of the forced mode into the gyration mode must generate a companion quasi-particle of energy $f_{\text{rf}} - f_g$ to conserve energy. We conclude that the first-to-occur scattering mechanism is thus very likely to be:

$$\underbrace{|\text{rf}\rangle}_{m=-1} \xrightarrow{\text{splitting}} \underbrace{|g\rangle}_{m=+1} + \underbrace{|\text{SB}^-\rangle}_{m=-2}, \quad (2)$$

where the exact nature and the azimuthal indices of the states $|\text{rf}\rangle$ and $|\text{SB}^-\rangle$ will be discussed below.

In related studies [18–20] the high frequency comb has been interpreted as the signature of Floquet states residing on a time-periodic gyrating vortex, with the frequencies reflecting the quasi-energies of the Floquet states. This previous interpretation is supported by two of our findings:

- At the crossing of the scattering threshold, the power of the gyration mode increases substantially (Fig. 2). The ground state on which the magnetic excitations reside ceases to be a non-coherently (thermally-driven) gyrating vortex and becomes a time-periodic gyrating vortex, supplying a Floquet context to the other eigenexcitations of the system.
- Correlatively, the regular eigenmodes of the static vortex that were easy to detect in sub-threshold regime

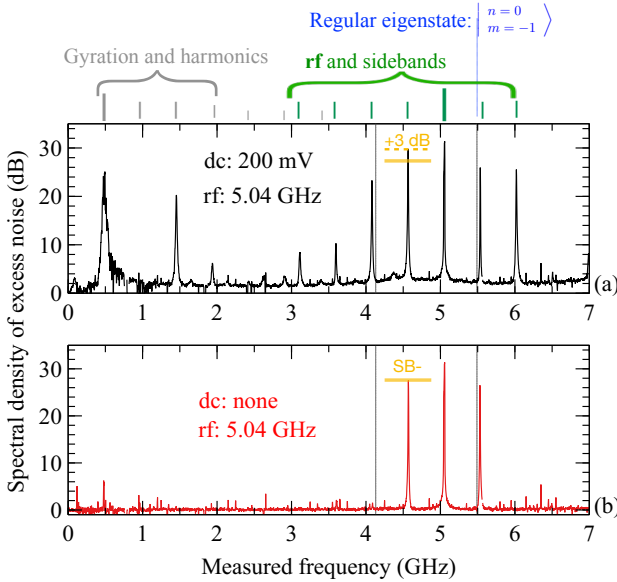


FIG. 3. Scattering of the forced $|rf\rangle$ mode into the gyration mode and resulting frequency comb for a 300 nm diameter device. Power spectral density when applying a pump at 5.04 GHz with a power of 10.8 dBm (a) in the presence of 200 mV of dc bias, and (b) in the absence of dc bias. The dashed yellow bar is the power threshold to be used later when analyzing the time-resolved amplitude of the first lower sideband SB^- .

(Fig. 1) disappear suddenly [Fig. 3(a)] and are replaced by the new spectral features with different frequencies, now being $f_{rf} + kf_g$, $k \in \mathbb{Z}$.

It is essential to assess whether the novel spectral features at $f_{rf} + kf_g$ correspond to *real* states with the same frequencies, or if these spectral features simply result from microwave mixing phenomena. This question is conveniently answered by setting $I_{dc} = 0$ because this suppresses the direct sensitivity to the modes while maintaining the mixing phenomena. Fig. 3(b) confirms that the gyration peak and the sidebands for $|k| > 1$ entirely [30] disappear from the spectra when the dc bias is suppressed. This proves that the spectral lines for $|k| > 1$ correspond to true states and that these states are populated. Conversely, the first lateral sidebands (i.e. $k = \pm 1$) do not vanish when the dc bias is suppressed: SB^- just decreases by 3 dB (see the yellow bars in the two panels of Fig. 3). It decreases but does not vanish simply because the large gyration maintains a relatively large mixing signal at this frequency (Eq. 1). Still, this reduction of the $|k| = 1$ sideband amplitudes is a proof of the existence of populated *real* states also for $k = \pm 1$.

We now discuss the dynamics of the scattering of the spin waves into the gyration (Eq. 2). For this we replace the spectrum analyzer by a single-shot oscilloscope [Fig. 1(a)] and analyze the transients of $V(t)$ after an

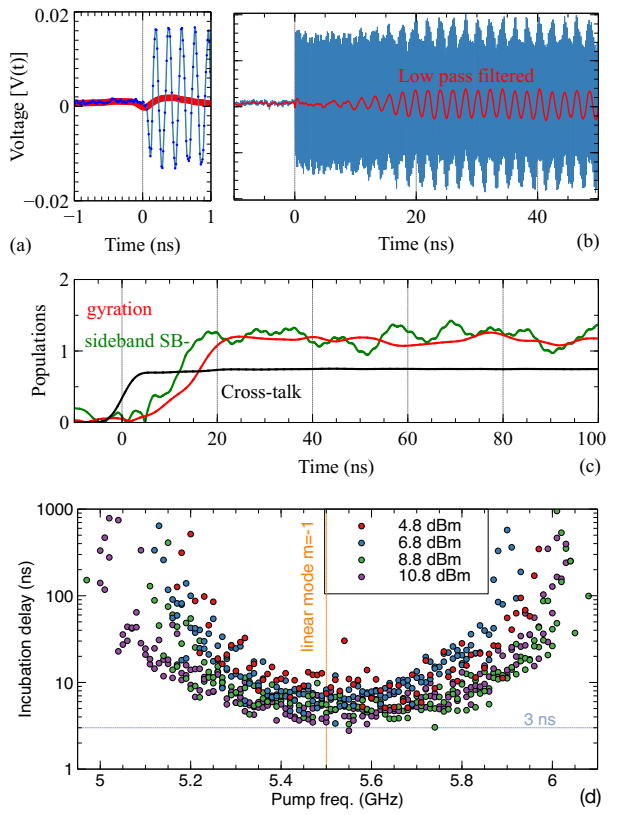


FIG. 4. Time-resolved population of the gyration mode for a 300 nm device. (a, b) $V(t)$ (blue) and a low-pass-filtered version of it (red) for a drive at $f_{rf} = 5.17$ GHz and 8.8 dBm with a dc bias of -200 mV. (c) Transients of the populations $n(t)$ of the gyration mode at $f_g = 492$ MHz (red, $\times 8$ magnification), of the Floquet mode of the lower sideband SB^- at $f_{rf} - f_g$ (green, $\times 60$ magnification) and of the signal at the forcing frequency f_{rf} (black). The oscillations in the population of SB^- originate from the experimental noise. (d) Dependence of the incubation delay of the gyration versus the pump frequency and the pump power. The vertical line is at the frequency of the regular eigenmode $|m = -1\rangle$.

abrupt application of the rf drive in the presence of a dc bias. A representative example of $V(t)$ is supplied in Fig. 4: in the first ns, $V(t)$ almost only reflects the cross-talk due to the fast-rising rf field at f_{rf} . Later, a smaller signal at the gyration frequency can be perceived as an added slower oscillation. To follow the population of the gyration and of the other modes, we performed a numeric I/Q demodulation of $V(t)$. The population n_f of a mode at a given frequency f scales with the modulus of the down-converted signal:

$$n_f(t) \propto \left| \mathcal{F}_{\text{low}}(V(t)e^{i2\pi ft}) \right| \quad (3)$$

where \mathcal{F}_{low} is a delay-free low-pass filter of cut-off frequency f_g . This value enables the separate tracking of the populations responsible for the individual sidebands, while maintaining a time resolution of $\pi/(2f_g) \approx 3$ ns

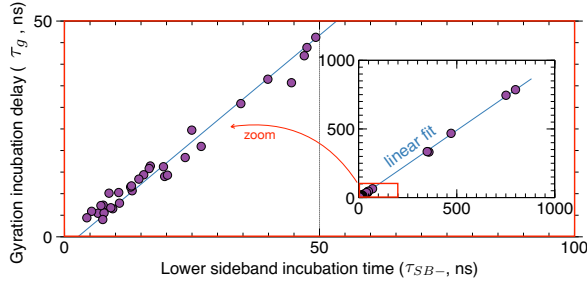


FIG. 5. Correlation between the incubation delays of the gyration and of the appearance of the signal of the lower sideband. Each point is a single shot event for applied frequencies spanning from 5 to 5.44 GHz, a power of 10.8 dBm and dc biases of -200 and +200 mV.

[31]. This demodulation procedure degrades the time-resolution of the populations $n_f(t)$ compared to that of the raw data $V(t)$, as evident when looking at the rise time of the demodulated amplitude of the cross-talk-dominated signal at f_{rf} [Fig. 4(c), black curve]. Note that the filter \mathcal{F}_{low} is delay-compensated, so as to maintain the time origin at $t = 0$ after the demodulation despite the degradation of the time resolution.

We clearly observe that a delay is needed for the gyration to reach its steady state amplitude [see Fig. 4(a)]. We thus define the "incubation delay" τ_g of the gyration as the time required to reach within 3 dB of its average steady state value. This delay τ_g fluctuates stochastically from event to event and can occasionally be as short as 3 ns [Fig. 4(d)]. The gyration incubation delay diverges when reaching the border of the scattering region of the $\{P_{\text{rf}}, f_{\text{rf}}\}$ space, as earlier displayed in Fig. 2.

The mean value of τ_g is clearly minimal when $f_{\text{rf}} = 5.5$ GHz, i.e. when the drive is resonant with the regular eigenmode $m = -1$ [see Fig. 4(d)]. The minimal τ_g is 3 ns; this value is a true delay, not an artefact of the finite time-resolution of the demodulation procedure. This dependence of τ_g with the carrier frequency bears some similarity with $1/\chi''(f)$, i.e. the inverse of the susceptibility of the $m = -1$ mode. This minimum of τ_g at $f_{|m=-1}$ indicates that the quasi-particle $|\text{rf}\rangle$ that scatters into the gyration mode is an off-resonantly excited $|m = -1\rangle$ regular eigenmode, confirming the speculation of Eq. 2. The forced mode $|\text{rf}\rangle$ that scatters and the gyrotropic mode $|g\rangle$ thus share the opposite azimuthal numbers. Since the total azimuthal number must be conserved in the scattering process [8], this scattering picture entails that the companion mode $|\text{SB}^-\rangle$ is a Floquet state of azimuthal character $m = -2$.

In this scattering picture expressed by Eq. 2, the companion quasi-particle of energy $f_{\text{rf}} - f_g$ should be emitted simultaneously with the gyration magnon. Let us check this by time-resolving the population of the Floquet mode $k = -1$ through the I/Q demodulation of the sideband SB^- . The $n_{\text{SB}^-}(t)$ curves [Fig. 4(c)] resemble

the ones of the gyration: they are step functions with incubation delays. To ensure that their incubation delays τ_{SB^-} reflect the *cumulated* growth of both the mixing part of the signal and the contribution of the population of the $k = -1$ Floquet mode, τ_{SB^-} is defined with an amplitude threshold set at 2 dB below our best estimation of the average steady state level of n_{SB^-} , chosen as $\langle n_{\text{SB}^-}(t \gg \tau_{\text{SB}^-}) \rangle$. This threshold was earlier displayed as the yellow dashed bar in Fig. 3: it is above the contribution of the sole microwave mixing part.

Despite the low signal to noise ratio and the resulting degraded time resolution, we can state that the growths of n_g and n_{SB^-} are synchronous and share a *common* incubation delay. To better evidence that despite its event-to-event variability this is a common delay, we show in Fig. 5 that there is a one-to-one correlation between the independently extracted τ_g and τ_{SB^-} . The $k = -1$ Floquet mode and the gyration mode are born simultaneously, such that the scattering is in fact a splitting.

In summary, our experiments demonstrate that when pumping a vortex dot with an in-plane rf magnetic field, the first-to-occur scattering mechanism is a splitting of a $|m = -1\rangle$ regular eigenmode into the pair formed by a gyration magnon and a Floquet spin wave. The scattering threshold and the scattering time are minimal when the $|m = -1\rangle$ regular eigenmode is resonantly excited. The appearance of the Floquet context related to the gyration ground state and of the Floquet spin wave is thus not an egg-and-chicken problem: the two are generated synchronously by the first-to-occur scattering process. The subsequent time evolution of the system is an unresolved problem that will deserve attention in the future. Notably of interest, there should be a cascade of scattering mechanisms that populate all the other Floquet modes responsible for all the other spectral sidebands. Besides, it would be interesting to determine the path taken by the firstly driven regular eigenstate to later evolve into, or be replaced by a Floquet mode of same azimuthal number when in the steady state regime.

We acknowledge financial support from the EU Research and Innovation Programme Horizon Europe under grant agreement n°101070290 (NIMFEIA). We thank L. Körber and J. H. Mentink from Radboud University for insightful discussions.

* thibaut.devolder@cnrs.fr

- [1] H. Yu, J. Xiao, and H. Schultheiss, Magnetic texture based magnonics, *Physics Reports Magnetic texture based magnonics*, **905**, 1 (2021).
- [2] T. Shinjo, T. Okuno, R. Hassdorf, K. Shigeto, and T. Ono, Magnetic Vortex Core Observation in Circular Dots of Permalloy, *Science* **289**, 930 (2000).
- [3] R. Hertel, S. Gliga, M. Fähnle, and C. M. Schneider, Ultrafast Nanomagnetic Toggle Switching of Vortex Cores,

Physical Review Letters **98**, 117201 (2007).

[4] B. Taurel, T. Valet, V. V. Naletov, N. Vukadinovic, G. de Loubens, and O. Klein, Complete mapping of the spin-wave spectrum in a vortex-state nanodisk, *Physical Review B* **93**, 184427 (2016).

[5] K. Schultheiss, R. Verba, F. Wehrmann, K. Wagner, L. Körber, T. Hula, T. Hache, A. Kákay, A. Awad, V. Tiberkevich, A. Slavin, J. Fassbender, and H. Schultheiss, Excitation of Whispering Gallery Magnons in a Magnetic Vortex, *Physical Review Letters* **122**, 097202 (2019).

[6] L. Körber, K. Schultheiss, T. Hula, R. Verba, J. Fassbender, A. Kákay, and H. Schultheiss, Nonlocal Stimulation of Three-Magnon Splitting in a Magnetic Vortex, *Physical Review Letters* **125**, 207203 (2020).

[7] L. Körber, C. Heins, T. Hula, J.-V. Kim, S. Thlang, H. Schultheiss, J. Fassbender, and K. Schultheiss, Pattern recognition in reciprocal space with a magnon-scattering reservoir, *Nature Communications* **14**, 3954 (2023).

[8] R. Verba, L. Körber, K. Schultheiss, H. Schultheiss, V. Tiberkevich, and A. Slavin, Theory of three-magnon interaction in a vortex-state magnetic nanodot, *Physical Review B* **103**, 014413 (2021).

[9] J. P. Park and P. A. Crowell, Interactions of Spin Waves with a Magnetic Vortex, *Physical Review Letters* **95**, 167201 (2005).

[10] K. Y. Guslienko, A. N. Slavin, V. Tiberkevich, and S.-K. Kim, Dynamic Origin of Azimuthal Modes Splitting in Vortex-State Magnetic Dots, *Physical Review Letters* **101**, 247203 (2008).

[11] S. Salama, J.-V. Kim, A. Anane, and J.-P. Adam, Large frequency nonreciprocity of azimuthal spin-wave modes in submicron vortex state disks, *Physical Review B* **111**, 134445 (2025).

[12] M. Kammerer, M. Weigand, M. Curcic, M. Noske, M. Sproll, A. Vansteenkiste, B. Van Waeyenberge, H. Stoll, G. Woltersdorf, C. H. Back, and G. Schuetz, Magnetic vortex core reversal by excitation of spin waves, *Nature Communications* **2**, 279 (2011).

[13] M.-W. Yoo and S.-K. Kim, Azimuthal-spin-wave-mode-driven vortex-core reversals, *Journal of Applied Physics* **117**, 023904 (2015).

[14] M. Sproll, M. Noske, H. Bauer, M. Kammerer, A. Gangwar, G. Dieterle, M. Weigand, H. Stoll, G. Woltersdorf, C. H. Back, and G. Schütz, Low-amplitude magnetic vortex core reversal by non-linear interaction between azimuthal spin waves and the vortex gyromode, *Applied Physics Letters* **104**, 012409 (2014).

[15] A. S. Jenkins, L. S. E. Alvarez, S. Memshawy, P. Bortolotti, V. Cros, P. P. Freitas, and R. Ferreira, Electrical characterisation of higher order spin wave modes in vortex-based magnetic tunnel junctions, *Communications Physics* **4**, 107 (2021).

[16] Z. Gao, F. Wang, X. Zhao, T. Wang, J. Hu, and P. Yan, Interplay between spin wave and magnetic vortex, *Physical Review B* **107**, 214418 (2023).

[17] Z. Wang, H. Yuan, Y. Cao, and P. Yan, Twisted Magnon Frequency Comb and Penrose Superradiance, *Physical Review Letters* **129**, 107203 (2022).

[18] C. Heins, L. Körber, J.-V. Kim, T. Devolder, J. H. Mentink, A. Kákay, J. Fassbender, K. Schultheiss, and H. Schultheiss, *Self-induced Floquet magnons in magnetic vortices* (2024), arXiv:2409.02583 [cond-mat].

[19] C. Heins, A. Kákay, J.-V. Kim, G. Hlawacek, J. Fassbender, K. Schultheiss, and H. Schultheiss, *Control of magnon frequency combs in magnetic rings* (2025), arXiv:2501.05080 [cond-mat].

[20] G. Philippe and J.-V. Kim, *Excitation of vortex core gyration in nanopillars through driven Floquet magnons* (2025), arXiv:2507.19865 [cond-mat].

[21] B. A. Ivanov and C. E. Zaspel, High Frequency Modes in Vortex-State Nanomagnets, *Physical Review Letters* **94**, 027205 (2005).

[22] F. Boust and N. Vukadinovic, Micromagnetic simulations of vortex-state excitations in soft magnetic nanostructures, *Physical Review B* **70**, 172408 (2004).

[23] T. Devolder, Using rf voltage induced ferromagnetic resonance to study the spin-wave density of states and the Gilbert damping in perpendicularly magnetized disks, *Physical Review B* **96**, 104413 (2017).

[24] N. Smith, Modeling of thermal magnetization fluctuations in thin-film magnetic devices, *Journal of Applied Physics* **90**, 5768 (2001).

[25] S. Shreya, A. S. Jenkins, Y. Rezaeiyan, R. Li, T. Böhnert, L. Benetti, R. Ferreira, F. Moradi, and H. Farkhani, Granular vortex spin-torque nano oscillator for reservoir computing, *Scientific Reports* **13**, 16722 (2023).

[26] A. S. Jenkins, L. Martins, L. C. Benetti, A. Schulman, P. Anacleto, M. S. Claro, I. Caha, F. L. Deepak, E. Paz, and R. Ferreira, The impact of local pinning sites in magnetic tunnel junctions with non-homogeneous free layers, *Communications Materials* **5**, 7 (2024), publisher: Nature Publishing Group.

[27] F. Bruckner, S. Koraltan, C. Abert, and D. Suess, *magnum.np*: a PyTorch based GPU enhanced finite difference micromagnetic simulation framework for high level development and inverse design, *Scientific Reports* **13**, 12054 (2023).

[28] J. Ding, G. N. Kakazei, X. Liu, K. Y. Guslienko, and A. O. Adeyeye, Higher order vortex gyrotropic modes in circular ferromagnetic nanodots, *Scientific Reports* **4**, 4796 (2014).

[29] Except when f_{rf} is directly resonant with the gyration mode, a situation that is not studied here.

[30] In fact, the rectification of I_{rf} by a synchronous variation of the device resistance generate a small dc current flowing through the MTJ, which renders the gyration observable in the spectra as a small narrow line at 480 MHz.

[31] The imperfect selectivity of \mathcal{F}_{low} in Eq. 3 leads to some spectral leakage of n_{rf} into the estimation of the populations for the $|k| = 1$ modes. This leakage affects $n_{SB}(t)$ only during the rise time n_{rf} and can be compensated by systematically subtracting a fixed fraction of $\frac{dn_{rf}}{dt}$ from Eq. 3 when estimating $n_{SB}(t)$.